

# Air-to-Ground Real-Time Multimedia Delivery: a Multipath Testbed

Manlio Bacco<sup>[0000-0001-6733-1873]</sup>, Pietro Cassarà<sup>[0000-0002-3704-4133]</sup>, and  
Alberto Gotta<sup>[0000-0002-8134-7844]</sup>

Institute of Information Science and Technologies (ISTI), National Research Council  
(CNR), Pisa, Italy; emails: `[name.surname]@isti.cnr.it`

**Abstract.** In this work, we focus our attention on real-time multimedia flows from Unmanned Aerial Vehicles (UAVs) to the ground, presenting and analysing the data collected in field trials during a real testbed. The objective is assessing whether a video feed of reasonable quality can be provided to the pilot of an UAV to enable Beyond Visual Line of Sight (BVLoS) operations, by exploiting the multiple cellular operators available in the area. Three cellular networks have been jointly used in a multihoming/multipath setup, leveraging the variable coverage offered in both urban and suburban environments. Taking into account both Quality of Service (QoS) and Quality of Experience (QoE) metrics, the target parameters measured in this testbed are: latency, packet error rate, and video quality, which accounts for frames integrity, continuity, and fluidity. Data collected on the field allow to evaluate both QoS and QoE in the presence of a multipath architecture, showing how the latter, in the presence of network diversity, offer the possibility to improve the QoE at the receiver. We also design a framework to characterize the error model and to map it into a QoE model, therefore providing an analytical characterisation of a multipath channel.

**Keywords:** multipath · video streaming · real-time · QoS · QoE · testbed

## 1 Introduction

The use of UAVs is increasingly common in a wide spectrum of applications and services [1]. Being connected flying objects that can carry things, connect to networks or provide connectivity, monitor areas, people, and buildings [2], UAVs can prove to be very versatile, fast-moving, and available in a large range of sizes. The use of UAVs as moving Radio Access Network (RAN) [3], especially in the case of 5G networks, is gaining popularity in the literature, and real testbeds have been already carried out demonstrating the feasibility of such an approach. UAVs are also commonly used for monitoring activities [4], among others, through video streaming given that high-resolution cameras, fitting also on small UAVs, are largely available on the market. In this line, use cases of interest, especially considering BVLoS flights, are those related to e.g., inspection of power lines [5] - with flights in the range of tens of kilometers - to spot points in

39 which intervention may be needed; inspection of infrastructure, such as railways  
 40 [6]; or in smart cities for the purposes of traffic monitoring and management,  
 41 health services, tourism, and goods delivery [7]. Air-to-ground video feedback is  
 42 a common solution in the absence of Visual Line of Sight (VLoS) [8].

43 This work considers scenarios, as those just mentioned, in which real-time  
 44 video streaming from UAVs to ground stations is needed, i.e., the case of latency-  
 45 sensitive applications and services. According to 5G classes of services, such sce-  
 46 narios would fall into Ultra-Reliable and Low Latency Communications (URLLC)  
 47 and enhanced Mobile BroadBand (eMBB) [9]. Further than latency sensitivity,  
 48 we consider as key requirement the QoE at the Ground Control Station (GCS),  
 49 aiming at supporting the pilot on the ground in the case of BVLoS flights. In  
 50 fact, it is most important that the pilot has visual feedback coming from the  
 51 UAV for safety and security reasons, and such feedback must be both reliable  
 52 and real-time.

53 We focus on urban and suburban areas, extending our previous contribution  
 54 in [10], targeting the provision of real-time *situational awareness* [11], requiring  
 55 minimal loss rate and low delay.

56 The results herein presented are based on a real testbed carried out in the  
 57 city of Pisa, Italy, and its suburban area. We exploit multiple Network Interface  
 58 Cards (NICs) at the sender - a multihoming setup - to maximise the probability  
 59 of always having at least one active link delivering the video flow to the GCS.  
 60 In fact, poorly served areas (as sometimes the case of suburban ones) may cause  
 61 the links to temporarily drop, as well as heavy traffic in others (as sometimes in  
 62 cities) may be the cause of an unacceptable large delay. Both situations are to  
 63 be avoided in a subcritical scenario as the one we consider, thus motivating us to  
 64 rely on multihoming to increase the probability of having at least one active link,  
 65 with reduced loss rate and contained delay. The use of different cellular networks  
 66 for air-to-ground multimedia delivery in our testbed means that redundant al-  
 67 ternative paths are in place between sender and receiver, thus increasing the  
 68 probability of achieving situational awareness. We use three sender-side NICs  
 69 for data transmission over three different public cellular networks, delivering  
 70 traffic to a single NIC on the ground, i.e., at the GCS. As highlighted in [12]  
 71 and actually experienced in our scenario, the various paths are not necessarily  
 72 disjoint, and this can depend on several reasons. In our testbed, it is likely that  
 73 some sections of the fixed infrastructure on the ground is shared among diffe-  
 74 rent operators in certain areas, meaning that the network QoS of the different  
 75 links may show non-negligible correlations. Eventually, this may impact on the  
 76 achievable QoE, as we show in this paper when mapping QoS into QoE.

77 Based on those premises, this work provides both a real implementation and  
 78 insights in: *(i)* the opportunistic use of the access networks of multiple cellular  
 79 Internet Service Providers (ISPs) to deliver a video stream from an UAV towards  
 80 a GCS in a real testbed; *(ii)* the use of multipath transport to improve the QoE  
 81 at the GCS; *(iii)* an analytical framework to characterise multipath communi-  
 82 cations; and, finally, *(iv)* the mapping of QoS statistics into QoE evaluations.  
 83 The rest of this paper is organized as follows: Section 2 surveys the state of the

84 art, focusing on scenarios similar to the one under consideration herein, and on  
 85 the use of multipath techniques to deliver multimedia live streams. Section 3  
 86 provides details on the system configuration used to carry out the testbed and  
 87 the related system parameters. Section 4 introduces to the analytical framework  
 88 proposed in this work, used to characterise the multipath channel and to support  
 89 the mapping of QoS into QoE, which is presented in Section 5. Finally, Section 6  
 90 draws the conclusions and opens to future works.

## 91 2 Related Works

92 In this section, we survey how key requirements of our scenario are approached  
 93 in the literature, what kind of solutions have been identified so far, and how and  
 94 why our approach is different from the other ones we consider.

### 96 2.1 Use cases and requirements for air-to-ground video feeds

97 A valuable recollection of use cases leveraging UAVs can be read in [13] -  
 98 focusing on Internet of Things (IoT) scenarios - covering for instance disaster  
 99 management, traffic monitoring, crowd surveillance, or environmental monitor-  
 100 ing [5] and agricultural applications [14]. In those scenario, the use of cellular  
 101 connections is typically foreseen, calling for an analysis of the quality of the  
 102 signal from above. In several studies, such as in [15,16], the quality of the sig-  
 103 nal has been evaluated at flying altitudes, showing that 4G connectivity can be  
 104 effectively used to provide wide-area wireless connectivity to UAVs [15], even  
 105 if limitations should be taken into account, like the rapid decrease of the re-  
 106 ceived signal as the altitude increases [16]. Thus, the possibility of using UAVs  
 107 in conjunction with terrestrial networks has been investigated in the literature  
 108 with positive results. What needs careful evaluation is the actual possibility of  
 109 achieving the so-called situational awareness in BVLoS conditions via public cel-  
 110 lular networks, which calls for careful attention to maximise the probability of  
 111 *video continuity*, which is one of our key requirements. Further than continuity,  
 112 the *playout delay*, i.e., the time delay after which a video chunk is played with  
 113 respect to its generation instant at the source side, must be strictly limited to  
 114 actually provide real-time visual context. Thus, a minimum value of playout  
 115 delay adds to the list of considered requirements in this work.

### 117 2.2 Multipath protocol solutions and real-time video streaming

118 Real-time video streaming poses additional requirements to those above. In the  
 119 case of multipath protocols - on which a valuable survey is available in [17] -  
 120 one of the first solutions available in the literature and actually implemented  
 121 is MultiPath TCP (MP-TCP) [18]. Its main advantage is bandwidth aggrega-  
 122 tion, contrarily to what the Stream Control Transmission Protocol (SCTP) does.  
 123 SCTP is a multihoming protocol using a single link at a time, whereas the other

link are backup options for reliability purposes. In the case of multimedia data delivery, MultiPath RTP (MP-RTP) [19] is the multipath version of RTP, the protocol designed for end-to-end, real-time transfer of streaming media. The available MP-RTP implementations provide additional features, such as the use of Forward Error Correction (FEC) techniques for congestion control [20] so to shift traffic from congested to less congested paths<sup>1</sup>. MultiPath QUIC (MP-QUIC) [22] can be cited as well as emerging multipath solution at the transport layer, offering encrypted, stream-multiplexed, and low-latency data exchanges. An emerging solution is the use of the DASH (Dynamic Adaptive Streaming over HTTP) protocol, which is TCP-based, also in the case of multipath solutions [23].

The core feature of multipath solutions is that disjoint paths between a sender and a receiver can be used as a single logical one to deliver data flows, leveraging network diversity to improve the link availability, increase the available bandwidth, or rely on several low-cost links to mimic the statistics provided by a single high-performance link. Those features can be alternative to each other or even partially achieved together; in our scenario, the aim is in improving the link availability to satisfy the requirement on video continuity. Typically, a key goal is the increase of available bandwidth, which anyway should be pursued by carefully choosing the links to be used to respect any latency constraints in the case of latency-sensitive applications. In fact, heterogeneous networks typically exhibit different network statistics, and multipath solutions may offer worse performance when compared with the plain protocol versions [19].

The use of MP-TCP has been tested for video streaming, as in [24, 25], i.e., using elastic protocols typically used in different scenarios, as for instance IoT ones [26]. Typically, real-time multimedia streaming does not occur over TCP because the constraint posed by live feeds makes unnecessary, if not even detrimental, the use of retransmissions in the presence of losses. In the case of elastic protocols, such as TCP, homogeneous paths (i.e., links showing comparable network statistics) represent a condition for satisfactory performance in multimedia streaming. In [12], the authors show how, on the one hand, constant bandwidth on multiple paths results in improved video quality with respect to the case of a single path; on the other hand, how bandwidth fluctuations harm user experiences. It must be noted that MP-TCP suffers from network middleboxes and proxies, thus its use may be limited or broken when traversing them. We excluded MP-TCP as a solution because of unneeded retransmissions, and to avoid potential issues with appliances on the ISPs networks that may impact on the desired QoE level. Real-time and high-quality video streaming is bandwidth-intensive and delay-sensitive [27], and has stringent QoS requirements. In fact, to really achieve real-time video streaming, a one-way delay of maximum 150ms

---

<sup>1</sup> A valuable survey on the topic of congestion for multipath protocols, including those for video streaming, can be read in [21].

164 should be taken into account<sup>2</sup>, as we do in this work. Other key requirements  
 165 on QoS are related to jitter and packet loss rate, which must be as contained  
 166 as possible for high-quality multimedia feeds. The use of FEC-based techniques  
 167 is a common approach to counteract loss phenomena. Nonetheless, FEC-based  
 168 multipath protocols in the literature are throughput-oriented and video data is  
 169 scheduled in a content-agnostic fashion [27], thus not making them the optimal  
 170 choice in the case of multimedia streaming. For instance, the work in [28]  
 171 proposes the use of a XOR-based dynamic FEC solution for MP-TCP to lower  
 172 the probability of retransmissions, thus reducing delays due to lost - and then  
 173 retransmitted - packets. Such a solution may be of some interest in the case  
 174 of latency-sensitive applications, but the use of FEC impacts on the TCP con-  
 175 gestion window - which defines how many bytes of data are sent per period -  
 176 because fresh data may be sacrificed in favor of redundancy. Furthermore, a sin-  
 177 gle loss is tolerated per FEC block in [28], a solution that, on the one hand, may  
 178 not be enough in the case of burst losses; but, on the other hand, provides low  
 179 computational overhead and a rather simple implementation. Burst losses is a  
 180 phenomenon that we experienced in our real tests, as shown below. It is also  
 181 worth highlighting that, the higher the FEC redundancy, the higher the energy  
 182 consumption [29]. Because of the occurrence of burst losses and of the need of  
 183 a simple but effective implementation to be run on constrained devices, we do  
 184 not rely on classical FEC approaches in this work. From the viewpoint of the  
 185 implementations, those in user-space - rather than at different layers of the stack  
 186 - are increasingly common because of the flexibility they can provide in different  
 187 scenarios [28], as we argued in [30] in the case of generic IoT traffic. We will  
 188 consider user-space solutions in future works for the flexibility they provide.

189 On a closing note, we briefly acknowledge that novel video coding schemes  
 190 have been proposed for high-quality video from UAVs to ground users because  
 191 existing ones do not yet meet the expected QoE according to [31]. In this work,  
 192 we exploit well-established solutions for video coding, such as the H.264 stan-  
 193 dard, relying instead on the use of a multipath setup to meet the desired QoE.  
 194 Multipath solutions provide advantages in the presence of network diversity, as  
 195 we show in the results. Our scenario is in high mobility conditions in both urban  
 196 and suburban areas. To strengthen the connection reliability, lightweight FEC  
 197 solutions are herein preferred to more resource-consuming ones, such as network  
 198 coding as proposed in similar cases [32].

199

### 200 2.3 The impact of QoS on QoE

201 Finally, we briefly cover the state of the art on how to map the network  
 202 statistics (i.e., QoS) into QoE, thus opening to sender-side scheduling strate-  
 203 gies that target a predefined QoS that can provide a QoE level above a prede-  
 204 fined threshold. QoE takes into consideration the end-user subjectivity, which

<sup>2</sup> ITU-T G.114 recommends a less than 150 millisecond one-way delay as excellent for media quality, although delays between 150 and 400 milliseconds are considered as still acceptable.

205 depends on QoS and other factors; consequently, subjective and objective qua-  
 206 lity assessment methods are needed to model the impact of both technical and  
 207 non-technical factors, as analysed in [33]. Several works [34–36] faced with the  
 208 definition of mapping QoS onto QoE. In [35, 36], the authors discuss learning  
 209 approaches for both online and offline mapping. All the proposed mappings  
 210 build on quality comparisons between the undistorted (source side) video and  
 211 the potential distorted (destination side) video, namely *reference* and *outcome*,  
 212 respectively. The quality of the outcome can be rated in terms of Mean Opinion  
 213 Score (MOS)<sup>3</sup> exploiting the reference. Whether the reference is available or not  
 214 defines the following types of metrics: Full Reference (FR), No Reference (NR),  
 215 and Reduced Reference (RR). In the case of FR, both subjective and objec-  
 216 tive comparisons of the outcome with the reference can be carried out because  
 217 both are available at destination. Hence, very accurate metrics can be derived. In  
 218 the case of NR, a quality score must be derived from the outcome only, which  
 219 of course provides poorer information if compared with the FR case. In a ty-  
 220 pical scenario, such as the one under analysis in this work, NR-based metrics  
 221 lack the possibility of discerning between pure quality-related issues from any  
 222 disturbances due to the network [35, 36]. But the obtained metrics can be esti-  
 223 mated through low-complexity algorithms, thus being suitable for online use in  
 224 resource-constrained and/or real-time settings. Man-in-the-loop’s feedback can  
 225 be collected at the sender in addition to network statistics in order to further  
 226 tune up NR metrics. RR must be considered as the case in between FR and NR  
 227 because of e.g., the availability of a QoE model or of data collected in similar  
 228 scenarios that can be used as reference. In other words, the core difference with  
 229 respect to NR is the possibility to exploit additional information at the destina-  
 230 tion to derive a more meaningful QoE metric. We make use of a QoE model in  
 231 this work, thus positioning our work in the RR case.

### 232 3 System Configuration

233 In this section, we describe the system configuration used in our real testbed,  
 234 briefly discussing the reference protocol stack in Section 3.1, the hardware setup  
 235 in Section 3.2, and the software setup in Section 3.4.

#### 236 3.1 Reference Protocol Stack

237 Multihoming consists in the capability of a device of leveraging a set of routes  
 238 provided by two or more ISPs, each one with a distinct IPv4/v6 address for both  
 239 inbound and outbound traffic. RFC 4116 details the IPv4 practices and goals of  
 240 a multihoming architecture that are:

- 241 – *redundancy*, which can protect a system from some single-point of failure  
 242 (SPOF). The degree of protection relies on the policies applied to intercon-  
 243 nect the system to the providers and how route the information on multiple  
 244 network interfaces;

<sup>3</sup> Recommendation ITU-T J.247, "Measurement of the quality of service. Objective perceptual multimedia video quality measurement in the presence of a full reference", 08/2008.

- 245 – *load sharing*, which account for how outbound traffic is shared across multiple
- 246 ISPs;
- 247 – *policies*, which accounts either for the capability of relaying certain types
- 248 of traffic to a given set of ISPs according to some budget rules or for path
- 249 scheduling according to certain QoS metrics;
- 250 – *simplicity and scalability* since multihoming solutions may require complex
- 251 algorithms that must not jeopardize but instead cope with the scalability of
- 252 a system.

253 UAVs-based solutions leveraging multihoming capabilities may also benefit of  
 254 multipath transport protocols, which can enable load sharing or concurrent  
 255 multipath transfer in multihomed systems. For end-to-end multimedia session,  
 256 multipath transport can provide several advantages over a single-path transmis-  
 257 sion, since it can provide higher transmission rate, redundancy between multiple  
 258 paths, and higher reliability.

259 However, multipath protocols require that the endpoints must implement  
 260 and support multipath transport. Establishing a multipath transport scenario  
 261 based on application-level relay (AR) is one of the multipath routing methods,  
 262 proposed in [37] as a general framework for multipath transport systems (MPTS-  
 263 AR). Figure 1 shows the protocol stack, which shifts the multipath management  
 264 to a shim-layer, which accounts for implementing the relay and redundancy  
 265 policies other than the multiple sessions establishment. MPTS-AR has several  
 266 advantages: *(i)* does not require any specific application/transport protocol to  
 267 work, *(ii)* does not require any modifications to the protocol stack to support  
 268 multipath capabilities, and *(iii)* opens to the use of different protocol flavors on  
 269 different paths. In this work, such a framework can be considered as a reference  
 270 one, which we implemented as later described.

### 271 3.2 Hardware Setup

272 In our setup, three onboard Long-Term Evolution (LTE) routers have been used  
 273 for multihoming, as shown in Figure 2b, which also zooms the Raspberry Pi  
 274 (RPi) used to collect and transmit the video feed.

275 The RPi 3 Model B+ is equipped with a Raspberry Pi Camera Module V2.1  
 276 for video streaming, and two USB WiFi dongles 2.4/5GHz, IEEE 802.11b/g/n  
 277 in addition to the integrated Broadcom BCM43438 wireless interface. Each WiFi  
 278 NIC is connected to a different LTE home-grade router Huawei E5573 4G-LTE  
 279 CAT4 with nominal download and upload rates of 150 Mbps and 50 Mbps, re-  
 280 spectively, so that three cellular connections may be used simultaneously during  
 281 the flight. The Huawei E5573 router can connect to clients via cable, Ethernet-  
 282 over-USB, or wireless. Each router is powered by a LiPo battery or through an  
 283 USB port. Also the RPi is powered through a powerbank visible below it in  
 284 Figure 2b, which allows the RPi to run for more than an hour, with a negligible  
 285 additional weight. In the presented setup, we preferred a wireless connection of  
 286 the RPi with the Huawei E5573 routers to reduce the impact on the powerbank,  
 287 and also to avoid any power surge on the USB bus of the RPi. The hardware

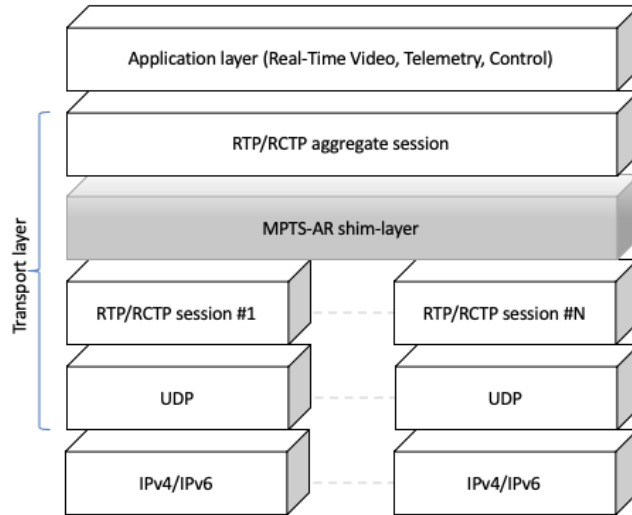


Fig. 1: RTP/UDP protocol stack used for multipath transport systems with application relay.



(a)



(b)

Fig. 2: The testbed platform in use: the UAV on the left, the RPi on top of a large capacity battery on the right, with the mounted Pi Camera Module, and three home-grade LTE routers.



288 visible in Figure 2b has been used as payload of the UAV into a red housing  
 289 visible in Figure 2a. The UAV is a custom octo-copter, already used in several  
 290 activities [2, 5, 14], weighting approximately 5 [Kg], equipped with brushless  
 291 engines, and able to fly at a maximum speed of 130 [Km/h] for about 15-20  
 292 minutes depending on the payload (up to 2.5 [Kg]). According to the definition  
 293 proposed in [38], such a configuration is similar to the so-called *tight plane-based*  
 294 *framework* used in smart cities.

295 At the receiver side, a laptop acts as GCS for both telemetry and live video  
 296 stream thanks to the open-source software *QGroundControl*. The receiver has  
 297 one public IPv4 address. For the sake of completeness, the laptop is based on  
 298 an Intel Core-i7 processor, 8GB RAM, running Ubuntu Linux. The RPi runs a  
 299 Raspbian Wheezy distribution. Furthermore, the three LTE routers are equipped  
 300 with SIM cards of three different Italian providers: Vodafone, Tim, and WindTre.

### 301 3.3 Network setup

302 Figure 3 shows the reference transmitting and receiving setup, as well as the use  
 303 of three cellular networks. Such a picture shows the three routing units detailed  
 304 in 3.2, which have a private IP number on different private networks, exemplified  
 305 with subnets 10.0.1.x, 10.0.2.x, and 10.0.3.x. Each ISP assigns a public IP to the  
 306 WAN port of the relative router. On the RPi, each NIC is configured with a  
 307 static IP address taken within the relative subnet of the relative router. An  
 308 *iptables* configuration was set, by using *Mangle* and *NAT* tables to manipulate  
 309 and forward the IP packets to the desired subnet according to the source address  
 310 and toward the same public destination address, i.e., that of the GCS (on the  
 311 right in Figure 3). Below we report the code to set up the IP forwarding rules  
 312 for subnet 10.0.1.x:

```
313 #!/bin/sh
314 receiver_udp_port=5000
315 wlan_if_1=wlx74da38c822ff
316 wlan_addr_1=10.0.1.103
317 gw_1=10.0.1.1
318 dst_port_1=5004
319
320 sudo iptables -t nat -D OUTPUT -p udp --dport $dst_port_1 -j DNAT
321     --to-destination :$receiver_udp_port
322 sudo iptables -t nat -D POSTROUTING -p udp -o $wlan_if_1 --dport
323     $receiver_udp_port -j SNAT --to-source $wlan_addr_1:$dst_port_1
324
325 sudo iptables -A OUTPUT -t mangle -p udp
326     --dport $dst_port_1 -j MARK --set-mark 4
327 sudo ip rule add fwmark 4 table SUBNET1
328 sudo ip route add default via $gw_1 dev $wlan_if_1 table SUBNET1
329 sudo iptables -t nat -A OUTPUT -p udp --dport $dst_port_1 -j
330     DNAT --to-destination :$receiver_udp_port
```

```

331 sudo iptables -t nat -A POSTROUTING -p udp -o $wlan_if_1
332     --dport $receiver_udp_port -j
333     SNAT --to-source $wlan_addr_1:$dst_port_1

```

### 3.4 Real-time video setup

GStreamer is a reference library for video streaming applications: it is an open source multimedia platform, available for the most common operating systems and embedded platforms, like the RPi. The release installed on both desktop and RPi for our experiments is version 1.14.4.

Our development efforts have been concentrated at the sender side, i.e. the platform onboard the UAV. A Gstreamer-based application is composed of a pipeline of software modules, called *plugins*, which implement the needed functional blocks, like encoding and decoding, mux and demux, buffering, scaling, dejittering, and data transport. In more details, the video stream is captured through the camera, scaled to a resolution of 1024x768 pixels at 10fps, and then compressed with an hardware-accelerated H.264 encoder. No adaptive video coding is used at the source, in order to account only for the impact of channel coding and channel erasures, or out-of-sequence packets. The video stream is parsed and encapsulated into Real-time Transport Protocol (RTP) packets, then the application relay (AR) enables the multipath feature: RTP packets are replicated on the respective paths to avoid SPOF. Such an implementation fulfills the goals in RFC 4116, i.e., it provides a lightweight implementation, suitable for constrained devices, achieving very low delay.

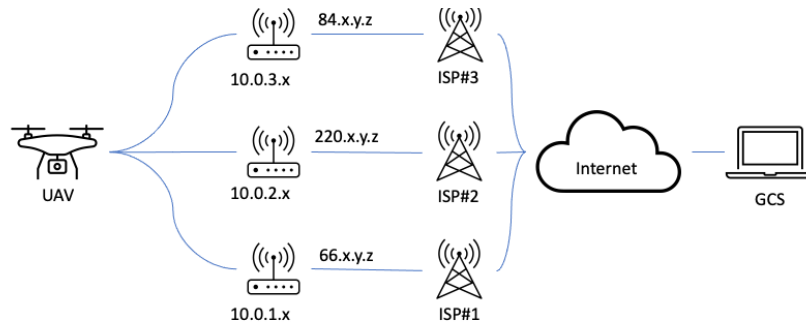


Fig. 3: Transmitting and receiving multipath/multihomed scheme for real-time multimedia flows from an UAV to a fixed GCS.

At the receiver side, a dejitter module - part of the Gstreamer pipeline - has been used to reorder and to remove duplicated packets, the latter likely to occur because of the replicas. The maximum allowed latency of the dejitter buffer is set to  $\mathcal{L}=0.2$  [s] in our setup, i.e., it handles out-of-sequence packets delayed up to  $\mathcal{L}$  [s]. Such a value is a reasonable tradeoff between piloting requirements and

358 varying network delay conditions when moving at medium-high speed with an  
 359 UAV. Table 1 summarises the values of the main parameters in use<sup>4</sup>.

360 The target Group of Pictures (GoP) size of the H.264 encoder is set to the  
 361 default GStreamer value of 90 frames. It translates into a high compression ratio,  
 362 but introducing large dependency among contiguous frames. The consequence is  
 363 that, in the case of a partially received video frame because of packet losses, also  
 the subsequent frames pertaining to the GoP are affected, lowering the QoE.

Plugin	Parameters
videosrc	video/x-raw, width = 1024 [px], height = 768 [px]
h264enc	target GoP size = 90, target-bitrate = 1 [Mbps]
rtph264pay	packet-size = 1432 [B], payload type 96
dejitter	latency = 200 [ms]

Table 1: System parameters of the GStreamer pipeline.

364

## 365 4 Analytical Framework

366 This section introduces the analytical error model for a multipath channel (in  
 367 Section 4.1) and the relative QoS metrics. The impact of the dejitter buffer is  
 368 discussed in Section 4.2, the main network statistics in Section 4.3, and the error  
 369 burst length in Section 4.4.

### 370 4.1 Multipath error model

371 We assume the channel model to be governed by a Discrete Time Markov Chain  
 372 (DTMC) at packet level as in [40], whose process is characterized by the evolution  
 373 of two states, *Good* ( $G$ ), and *Bad* ( $B$ ). We assume that no packet is lost being in  
 374  $G$ , while all packets are lost being in  $B$ . The DTMC model captures the bursty  
 375 nature of lossy periods with respect to a Bernoulli model, which cannot model  
 376 the burstiness of wireless and mobile channels. The channel transition of the  
 377  $i$ -path is described by the following transition matrix:

$$T_i = \begin{pmatrix} P_{GG,i} & P_{GB,i} \\ P_{BG,i} & P_{BB,i} \end{pmatrix},$$

378 where  $P_{X,Y,i}$  is the transition probability from state  $X$  to state  $Y$  in a period of  
 379 time equal to the transmission time  $T_p$  of a packet. From the DTMC theory, it  
 380 occurs that:

$$P_{GG,i} = 1 - P_{GB,i}, P_{BB,i} = 1 - P_{BG,i}.$$

<sup>4</sup> The testbed is driving us into the development of a simulator to further investigate the impact of said parameters and to further optimise the sender-side scheduling [39].

381 The average packet loss rate can be expressed as:

$$P_{BAD,i} = \frac{P_{GB,i}}{P_{GB,i} + P_{BG,i}}, \quad (1)$$

382 and the average error burst length  $abl_i$  as:

$$abl_i = \frac{1}{P_{BG,i}} = \frac{1}{1 - P_{BB,i}}. \quad (2)$$

383 In the case of two independent paths characterized by G/B channel states, the  
 384 aggregate behavior of the two paths can be described by means of a four-state  
 385 DTMC, where  $(G_1, G_2)$  is the first state,  $(G_1, B_2)$  the second one,  $(B_1, G_2)$  the  
 386 third one, and  $(B_1, B_2)$  the last one. In a multipath case with two paths, the  
 387 transition matrix  $T_{2-mp}$  of the four-states DTMC can be expressed, under the  
 388 hypothesis of independence of the  $i, j$  channels, as:

$$T_{2-mp} = \begin{pmatrix} P_{GG,1}P_{GG,2} & P_{GG,1}P_{GB,2} & P_{GB,1}P_{GG,2} & P_{GB,1}P_{GB,2} \\ P_{GG,1}P_{BG,2} & P_{GG,1}P_{BB,2} & P_{GB,1}P_{BG,2} & P_{GB,1}P_{BB,2} \\ P_{BG,1}P_{GG,2} & P_{BG,1}P_{GB,2} & P_{BB,1}P_{GG,2} & P_{BB,1}P_{GB,2} \\ P_{BG,1}P_{BG,2} & P_{BG,1}P_{BB,2} & P_{BB,1}P_{BG,2} & P_{BB,1}P_{BB,2} \end{pmatrix}. \quad (3)$$

389 Then, the stationary state probability distribution is:

$$\pi = \begin{pmatrix} (1 - P_{BAD,1})(1 - P_{BAD,2}) \\ (1 - P_{BAD,1})P_{BAD,2} \\ P_{BAD,1}(1 - P_{BAD,2}) \\ P_{BAD,1}P_{BAD,2} \end{pmatrix}. \quad (4)$$

390 Thus, a packet duplicated on both paths is lost if both the channels are in the  
 391 respective  $B$  states, that is:

$$P_{BAD,2-mp} = P_{BAD,1}P_{BAD,2}. \quad (5)$$

392 Analogously to Eq. (2), the resulting error burst length  $abl_{2-mp}$  of the four-state  
 393 DTMC can be expressed as:

$$abl_{2-mp} = \frac{1}{1 - P_{BB,1}P_{BB,2}}. \quad (6)$$

394 In the case of  $s$  paths, the DTMC is composed of  $2^s$  states and the resulting  
 395  $P_{BAD,s-mp}$ ,  $abl_{s-mp}$  are given by:

$$P_{BAD,s-mp} = \prod_{i=1}^s P_{BAD,i} \quad (7)$$

396

$$abl_{s-mp} = \frac{1}{1 - \prod_{i=1}^s P_{BB,i}} \quad (8)$$

397 It is worth nothing that, even relaxing the hypothesis of independence among the  
 398  $s$ -channels in Eq. (7), the product of  $P_{BAD,i}$  is replaced by the joint stationary  
 399 probability of having all the  $s$  channels in B state. Analogously for the  $egl_{s-mp}$ ,  
 400 the product of the  $P_{BB,i}$  is replaced by the joint transition probability that all  
 401 the  $s$  channels remain in B state. Under the hypothesis of independence, it is  
 402 easy to infer that  $P_{BAD,s-mp} \xrightarrow{s \rightarrow \infty} 0$  and  $egl_{s-mp} \xrightarrow{s \rightarrow \infty} 1$ . Contrarily, a strong  
 403 correlation between two paths or more implies that one of the two channels is  
 404 not providing any significant advantages in terms of network diversity.

## 405 4.2 Analysis of the Dejitter Buffer

406 The dejitter buffer is typically used in the presence of multimedia flows to reduce  
 407 the impact of jitter, so feeding the decoder in evenly spaced intervals despite the  
 408 irregularities due to the network. Its contribution is twofold in our case: on the  
 409 one hand, it allows for reordering out-of-sequence packets and for discarding  
 410 duplicated packets; on the other hand, the dejitter buffer drops packets sitting  
 411 in the queue longer than  $\mathcal{L}$  [s].

412 Because of such a behaviour, the dejitter buffer may contribute to the packet  
 413 loss rate as seen by the H.264 decoder with:

$$P_{drop} = P(\Delta D > \mathcal{L}), \quad (9)$$

414 where  $\Delta D$  is the delay between the arrival time of the out-of-order packet X  
 415 and the instant in which the reordering is successful because the packets be-  
 416 fore X have all been correctly received. If it takes less than  $\mathcal{L}$  to receive the  
 417 missing packets (successful reordering), then the out-of-order packet is correctly  
 418 forwarded; otherwise (unsuccessful reordering) it is dropped. Therefore, dropped  
 419 out-of-sequence packets contribute to  $P_{drop}$ .

420 The resulting loss rate seen by a H.264 decoder is given by Eqs. (7) and (9)  
 421 as<sup>5</sup>:

$$P_{loss} = P_{BAD,s-mp} + (1 - P_{BAD,s-mp})P_{drop}, \quad (10)$$

422 considering that only packets correctly received (with rate  $1 - P_{BAD,s-mp}$ ) can  
 423 be discarded because of  $\Delta D > \mathcal{L}$ .

## 424 4.3 Network statistics in experimental trials

425 This section describes how the measurement campaign has been conducted and  
 426 provides the statistical analysis of the collected QoS parameters. The experimen-  
 427 tal testbed involves an urban and a suburban route, which are shown separately  
 428 in Figure 4 to highlight the higher density of the Evolved Nodes B (eNBs) in  
 429 the urban part (see Figure 4b) than in the suburban part (see Figure 4a). Fur-  
 430 thermore, the suburban part considers uphill location, thus providing cellular  
 431 connectivity in Line of Sight (LoS) conditions with several distant eNBs. In our

<sup>5</sup> As in the case of Eq. (7), also Eq. (10) is applicable if the delay process on each of the  $s$  paths is assumed as independent from the other ones.

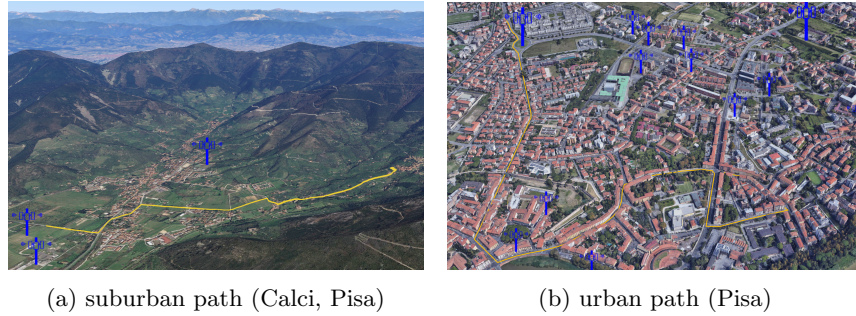


Fig. 4: 3D maps of the real testbed. The path is marked in yellow, the eNBs in blue.

432 testbed, the main constraint while moving was the availability of cellular con-  
 433 nectivity. The traffic at both the transmitter and the receiver has been dumped  
 434 thanks to the use of Tshark (an open-source network protocol analyzer) to sup-  
 435 port the following analysis. In the following, we present the one-way delay and  
 436 the latency accumulated by packets sitting in the de jitter buffer.

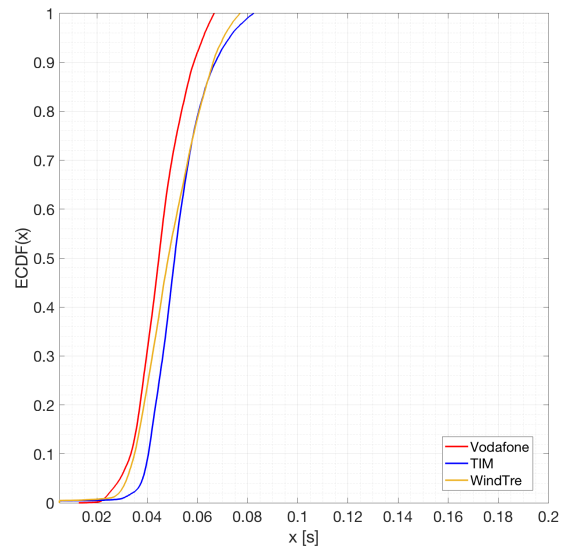
437 Figure 5 shows the one-way delay of each network.

438 It is shown for both suburban and urban scenarios in Figures 5a and 5b,  
 439 respectively. It is worth noting that both Tim and Vodafone operators share a  
 440 similar average value ( $\approx 30\text{-}40\text{ms}$ ) most of the time in the urban scenario, while  
 441 WindTre shows a different behaviour. All the operators behaves in a very similar  
 442 way in the suburban scenario.

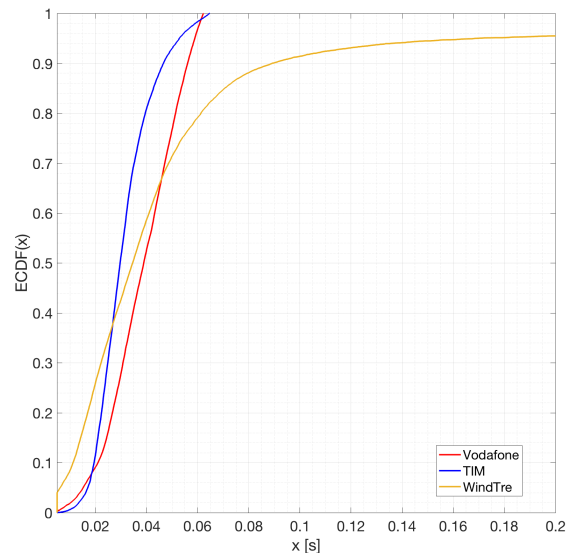
443 Figure 6 shows the survivor function of the delay accumulated by out-of-  
 444 sequence packets: the de jitter buffer forwards the first-come copy of each packet  
 445 (using the Sequence Number (SN)). However, different paths are likely to intro-  
 446 duce different latencies, as shown in Figure 5. Taking into account the maximum  
 447 tolerated latency  $\mathcal{L}$ , there is a non-null probability that the accumulated latency  
 448 may exceed such a value, as shown in Figure 6.

449 Table 2 shows the traffic share among the three operators, i.e., which fraction  
 450 of the data used by the H.264 decoder comes from Vodafone, Tim, or WindTre,  
 451 respectively. The testbed in the urban scenario confirms that the packets deliv-  
 452 ered by WindTre had experienced a lower one-way delay than the other two  
 453 operators. However, the sharing among the operators remains relatively fair be-  
 454 cause the distributions of the one-way delays are comparable. Regarding the  
 455 suburban scenario, the distributions of the one-way delays are almost identical  
 456 and this is reflected by the almost perfect sharing ratio among the operators.

457 The cumulative distribution functions (CDFs) of the receiving packet rate  
 458 for the suburban and urban scenarios are shown in Figures (7a) and (7b), respec-  
 459 tively. As discussed throughout this section, the three operators in the suburban  
 460 scenario exhibit the same performance level, while in the urban one they do  
 461 not. More precisely, CDFs of the suburban scenario show that the packet rates  
 462 never go below  $15 - 20$  [*pckts/sec*]. Instead, in the urban scenario, this is verified



(a) suburban scenario



(b) urban scenario

Fig. 5: Empirical Cumulative Distribution Function (ECDF) of the one-way delay.

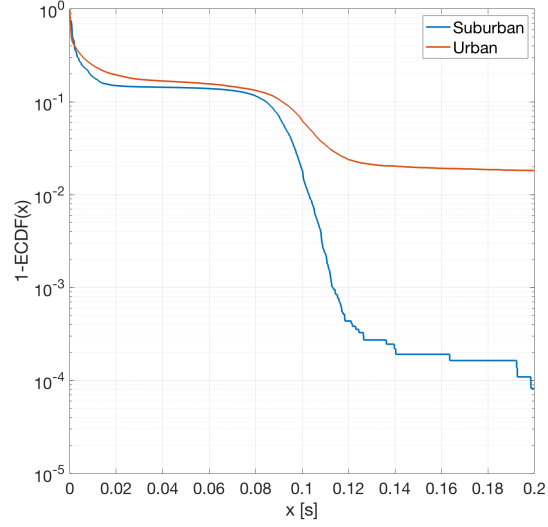


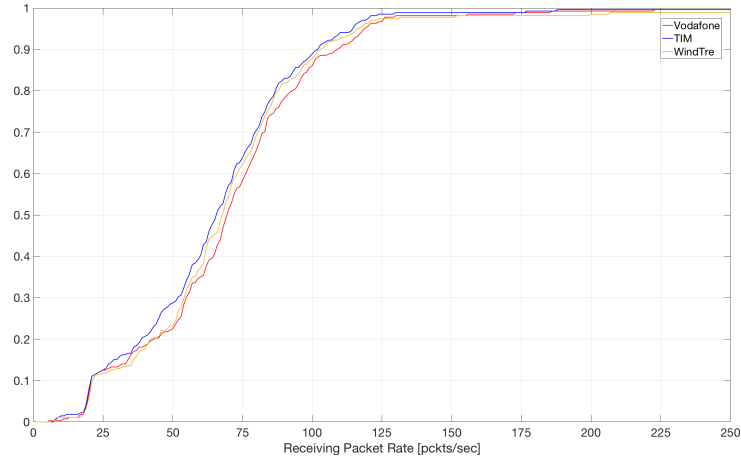
Fig. 6: Empirical survivor function of the latency accumulated by out-of-sequence packets in the dejitter buffer.

<b>scenario</b>	<b>operator</b>	<b>traffic sharing</b>
U	Tim	0.3039
U	Vodafone	0.3309
U	WindTre	0.3651
SU	Tim	0.3203
SU	Vodafone	0.3398
SU	WindTre	0.3398

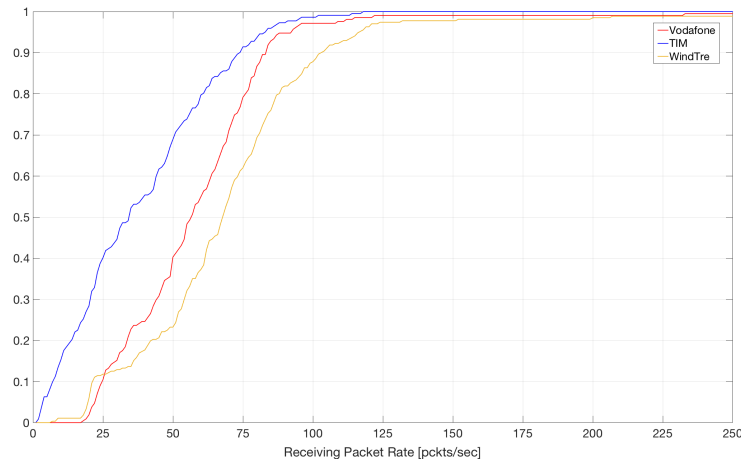
Table 2: Fraction of received traffic via each cellular network (after the dejitter buffer).



463 only in the case of Vodafone and WindTre, but not of TIM. Finally, the average  
 464 packet rate of the suburban scenario is similar for the three operators and falls  
 465 within the range  $60 - 70$  [pkts/sec], while in the urban scenario, WindTre and  
 466 Vodafone have an average rate in the range  $60 - 65$  [pkts/sec]. Instead, TIM  
 467 has a lower value, i.e., in the order of  $40 - 45$  [pkts/sec].



(a) suburban scenario



(b) urban scenario

Fig. 7: Cumulative Density Function (CDF) of the received bandwidth in packets (RTP/UDP) per second for both suburban and urban scenarios.

468 The error loss processes experienced on each path in both the scenarios are  
 469 in Table 3: they report the underlying DTMC processes as estimated from the

470 dataset. In addition, Table 3 reports the estimated DTMC process as seen after  
 471 the dejitter buffer, i.e. after multiplexing, reordering, and filtering of the three  
 flows.

scenario	operator	$T_i$	$\Pi_i$
U	Vodafone	$\begin{pmatrix} 0.9965 & 0.0035 \\ 0.0294 & 0.9706 \end{pmatrix}$	$\begin{pmatrix} 0.8944 \\ 0.1056 \end{pmatrix}$
U	WindTre	$\begin{pmatrix} 0.9997 & 0.0003 \\ 0.0185 & 0.9815 \end{pmatrix}$	$\begin{pmatrix} 0.9879 \\ 0.0121 \end{pmatrix}$
U	Tim	$\begin{pmatrix} 0.9783 & 0.0217 \\ 0.0999 & 0.9001 \end{pmatrix}$	$\begin{pmatrix} 0.8216 \\ 0.1784 \end{pmatrix}$
U	Aggregated	$\begin{pmatrix} 0.9818 & 0.0182 \\ 0.9816 & 0.0184 \end{pmatrix}$	$\begin{pmatrix} 0.9818 \\ 0.0182 \end{pmatrix}$
SU	Vodafone	$\begin{pmatrix} 0.9997 & 0.0003 \\ 0.5455 & 0.4545 \end{pmatrix}$	$\begin{pmatrix} 0.9994 \\ 0.0006 \end{pmatrix}$
SU	WindTre	$\begin{pmatrix} 0.9997 & 0.0003 \\ 0.5455 & 0.4545 \end{pmatrix}$	$\begin{pmatrix} 0.9994 \\ 0.0006 \end{pmatrix}$
SU	Tim	$\begin{pmatrix} 0.9881 & 0.0119 \\ 0.1932 & 0.8068 \end{pmatrix}$	$\begin{pmatrix} 0.9421 \\ 0.0579 \end{pmatrix}$
SU	Aggregated	$\begin{pmatrix} 0.99988 & 0.00012 \\ 0.99974 & 0.00026 \end{pmatrix}$	$\begin{pmatrix} 0.99992 \\ 0.00008 \end{pmatrix}$

Table 3: Transition matrices and stationary probabilities, after the dejitter buffer, of the empirical DTMC model of the channels of the three operators in the urban (U) and suburban (SU) scenarios, as well as the resulting *aggregated* channel.

472

#### 473 4.4 Error burst length

474 The error burst length  $abl$  can be calculated using Eq. (8), which provides the  
 475 values of 7 [pkts] and of 1.2 [pkts] before the dejitter buffer, and 1.018 [pkts] and  
 476 1.000 [pkts] after the dejitter buffer for the urban and suburban case, respectively.  
 477 The differences in the error burst lengths capture the intrinsic decorrelating  
 478 nature of a multipath system that not only works in difference of space, but  
 479 also of time. In fact, different delays are experienced by the replicas in different  
 480 paths. This effect significantly contributes in reducing the error correlation on  
 481 consecutive RTP packets within the dejitter buffer. According to Eq. 2 in [41],  
 482 the resulting one-step-correlation  $\rho$  between two consecutive packets in a DTMC  
 483 is given by:

$$\rho = P_{BB} + P_{GG} - 1, \quad (11)$$

484 Therefore, the resulting  $\rho_i$  for both urban (U) and suburban (SU) cases are  
 485 respectively calculated as:  $\rho_U = 0.832$  and  $\rho_{SU} = 0.152$ . By solving the equation  
 486 system composed of Eqs. (7), (8), and (11), the error burst length  $abl_i$  can be

487 expressed in terms of  $P_{BAD,i}$  and  $\rho_i$  as:

$$488 \quad ebl_i = \frac{1}{(1 - \rho_i)(1 + P_{BAD,i})}, \quad (12)$$

489 which fully characterizes the error process paired with Eq. (10) [42]. In fact,  
490 limiting  $\rho$ , i.e., reducing the burstiness of error sequences on packets, translates  
into the need for lower redundancy to protect the information [41].

## 491 5 Mapping Quality of Service into Quality of Experience

492 In the use case under consideration, quantifying the feeling of a remote operator  
493 about the received video feedback, in terms of QoE, becomes crucial towards the  
494 mapping of the latter with respect to QoS. A reference metric used to measure  
495 the feeling of a user about a video is based on MOS evaluations, performed  
496 using the statistical inference on the opinion scores, usually within a five-point  
497 interval, such as  $\{bad, poor, fair, good, excellent\}$ . QoE can be affected by video  
498 artifacts, missing frames, poor fluidity, and so on, which mainly depend from QoS  
499 parameters such as packet loss, delay, jitter, and maximum tolerable latency.

### 500 5.1 Analytical model

501 In [43, 44], the authors discuss the results of a metric, suitable for mobile net-  
502 works, which maps QoS into QoE as follows:

$$QoE = k_1 - \frac{k_2}{1 + (\frac{k_3}{Q})^\eta}, \quad (13)$$

with  $k_1, k_2$  defining the maximum and the minimum value of QoE, with  $Q$  and  $\{k_3, \eta\}$  instead depending on both network QoS and used video encoder. The model in Eq. (13) is also adopted in [45] to analyse the mapping between QoS and QoE in a video streaming scenario, where QoS is assumed to be a function of the loss rate; we adhere to the same assumption in what follows. The parameter  $Q$  in Eq. (13), which is the Non-Decodable Frame Rate, is defined as the complementary of that in [46], which is the ratio of the number of non-decodable frames to the total number of frames sent by a video source. The works in [45, 46] analyse scenarios in which a sequence of interdependent MPEG-based encoded frames are transmitted (as in our case), assuming that the propagation of the spatial error due to packet loss impacts on the frames that are dependent on a given previous frame. The MPEG streams are sequences of GoPs, which in turn are sequences of I, P, and B frame types. The loss of even a single packet may cause a video frame to be undecodable, according to [45, 46]. In turns, it means that I frames in a GoP are successfully decoded only if all packets are correctly received. A P frame is decodable only if the preceding I or P frames are successfully decoded and the packets delivering the P frame are successfully received. Finally, the B frames in a GoP are decodable only if the preceding and

succeeding I or P frames are both successfully decoded and all the B packets are successfully received. Hence, in the case of MPEG-based video, the expected Q value can be analytically evaluated as a function of the loss rate:

$$Q = 1 - \frac{N_{dec}}{N_I + N_P + N_B} \quad (14)$$

$$N_{dec} = N_{dec_I} + N_{dec_P} + N_{dec_B}$$

503 where the summation at the denominator is the total number of the I, P and B  
 504 frames that compose the video flow, and the numerator is the the number of the  
 505 successfully decoded frames. The number of decodable I, P and B frames can be  
 506 evaluated as:

$$N_{dec_I} = (1 - P_{loss})^{\bar{I}} N_{GoP} \quad (15)$$

507

$$N_{dec_P} = (1 - P_{loss})^{\bar{I}} N_{GoP} \sum_{i=1}^{n_P} (1 - P_{loss})^{i \cdot \bar{P}} \quad (16)$$

$$N_{dec_B} = [(1 - P_{loss})^{\bar{I} + n_P \bar{P}} + \sum_{i=1}^{n_P} (1 - P_{loss})^{i \cdot \bar{P}} (1 - P_{loss})^{\bar{B}}] \\ (M - 1)(1 - P_{loss})^{\bar{I} + \bar{B}} N_{GoP} \quad (17)$$

508 where  $N_{GoP}$  is the number of GoPs in the video flow;  $\bar{I}$ ,  $\bar{P}$  and  $\bar{B}$  are the average  
 509 number of packets composing frames I, P and B in a GoP, respectively;  $n_P$  and  
 510  $n_B$  are the average numbers of P and B frames in a GoP, respectively; and  $M - 1$   
 511 is the average number of B frames between I-P or P-P frames. Table 4 shows  
 512 the results coming from our testbed, highlighting that only I and P frames were  
 in use.

	Frame Type		
	I	P	B
<b>Avg. frames per GoP</b>	1	55	0
<b>Avg. RTP packets per frame</b>	10	6	0

Table 4: Average real GoP size (our testbed).

513

## 514 5.2 Testbed results

515 In this section, we provide the evaluation of the perceived video quality at the  
 516 GCS, according to Peak Signal-to-Noise Ratio (PSNR), Structural SIMilarity  
 517 (SSIM), and MOS evaluations [47]. The values can be read in Table 5. The  
 518 PSNR and SSIM metrics have been calculated for each operator and juxtaposed  
 519 to the aggregated multipath flow to highlight the advantages provided by the  
 520 use of a multipath setup.

As a premise, it is worth noting that the proposed multipath approach achieves at least a performance level equal to that of the most performing single path. This effect can be seen in Table 3, which, as explained above, shows the results obtained for the channel models of the considered network operators. In detail, in the urban scenario, the stationary probability of being in the BAD state for the multipath case (*Aggregated*) is comparable with that of the best performing operator (WindTre). However, looking at the transition matrix, the transition probability from BAD to GOOD is significantly increased; it can be explained by a contained improvement of the video quality since the probability of no transmission errors is increased. In the suburban case, the stationary probability of being in the BAD state in the multipath case is one order lower (0.00008) than that of a single path (WindTre is 0.0006), as well as the transition probability from BAD to GOOD has increased. A multipath setup contributes in decreasing the probability of the channel of being in the BAD state thanks to the path diversity: in fact, the probability that each path is simultaneously in a BAD state is much lower, as shown in Eq. (7). In other words, it is rather likely that at least one path can properly support the video delivery. The performance improvement due to a multipath setup is also reflected in the video quality statistics, as shown in Table (5). Such results show that multipath in the suburban scenario brings a reduced improvement over the best performing operator WindTre, which already provides excellent performance in terms of MOS, SSIM, and PSNR. Differently, a significant improvement is visible in the urban scenario, in which the multipath provides better video quality than each single link. An evident quality improvement, comparing the urban case with the suburban one, can be also seen in Figures (7a) and (7b), in which path diversity in the suburban case is evidently less pronounced than in the urban one.

operator	bad/poor	fair	good/excellent	avg PSNR	avg SSIM	MOS
(U) Vodafone	7.1%	2.4%	90.5%	46.85	0.86	good
(U) WindTre	6.9%	0.7%	92.4%	45.49	0.88	good
(U) Tim	41.8%	0.7%	57.5%	33.23	0.59	poor
<b>(U) Aggregated</b>	7.0%	0.3%	92.7%	47.6	0.93	excellent
(SU) Vodafone	7.0%	2.3%	90.7%	46.93	0.90	good
(SU) WindTre	11.9%	0.1%	88.0%	47.41	0.92	excellent
(SU) Tim	18.0%	1.0%	81.0%	43.14	0.82	good
<b>(SU) Aggregated</b>	6.3%	0.1%	93.6%	47.46	0.92	excellent

Table 5: Statistics on the per-frame video quality based on PSNR [dB] (5th column) and SSIM (6th column) metrics in both urban (U) and suburban (SU) scenarios. The 2nd, 3rd, and 4th columns report the shares of video frames per opinion score. A subjective evaluation is shown in the last column according to the UAV pilot.

Furthermore, we map QoS into QoE according to Eq. (13). In this respect, we rely on PSNR only (thus neglecting SSIM) in order to be coherent with the

549 model in Eqs. (15), (16), and (17). Table 6 reports the mapping among MOS,  
 550 PSNR, and  $P_{loss}$  calculated as follows: given the mapping between the MOS  
 551 evaluations and the PSNR values in Table 5, we derive the PSNR ranges for  
 given MOS value as in Table 6. Then, the video feeds have been fragmented to

MOS	bad	poor	fair	good	excellent
PSNR (dB)	< 20	$\geq 20$ < 30	$\geq 30$ < 40	$\geq 40$ < 50	$\geq 50$
$P_{loss}$	$\geq 0.25$	$\geq 0.2$ < 0.25	$\geq 0.1$ < 0.2	$\geq 0.05$ < 0.1	< 0.05

Table 6: Mapping MOS evaluation into PSNR values with respect to  $P_{loss}$ .

552 obtain short video sections each exhibiting only PSNR values falling into one of  
 553 the five MOS intervals. In this way,  $P_{loss}$  can be calculated and mapped with  
 554 the average PSNR value per video fragment; the results of such a procedure can  
 555 be read in Table 6. This mapping has been used to determine the two thresholds

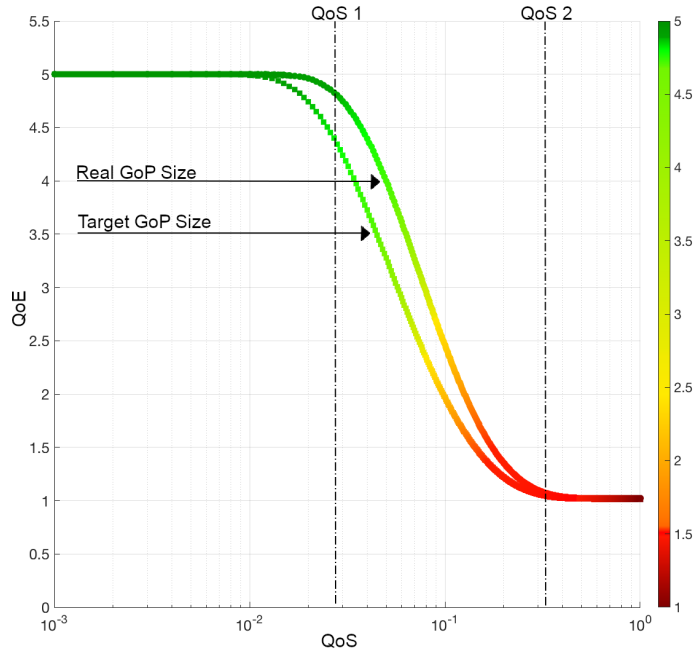


Fig. 8: Mapping QoS into QoE as a function of the  $P_{loss}$  parameter: target GoP size versus real (measured) GoP size.

557  $QoS_1$  and  $QoS_2$  shown in Figure 8 and presented in what follows. Referring to  
 558 Eq. (13), the parameters to be estimated are:  $k_1$ , set to the maximum QoE value  
 559  $k_1 = 5$ ;  $k_2$ , set to the minimum QoE value  $k_2 = 1$ ;  $\eta$ , which determines the slope  
 560 of the curve in Fig. 8; and  $k_3$ , which is related to both the difference  $k_2 - k_1$  and  
 561 the slope of the curve. Hence, determining the thresholds  $[QoS_1, QoS_2]$  limits  
 562 the range of values within which the parameter  $\eta$  can be chosen; the same goes  
 563 for the parameter  $k_3$ , which also depends on  $k_2 - k_1$  as said before. The derived  
 564 values are:  $k_2 = 990$ ,  $k_3 = 1.1818$ , and  $\eta = 33$ . Thus, Figure 8 shows the relative  
 565 mapping of the QoS into QoE, with the QoS degrading when moving from  $QoS_1$   
 566 to  $QoS_2$ . The region of very high QoE (excellent), up to  $QoS_1$ , represents the  
 567 case of a slight degradation of QoS with negligible effects on QoE. When the  
 568 QoS degradation falls within  $[QoS_1, QoS_2]$  (i.e., the second region), QoE start  
 569 decreasing (ranging from good to poor). Finally, once passed the threshold  $QoS_2$   
 570 (third region), the QoE should be considered as bad, that is, unacceptable QoE  
 571 causing users to give up on the service. According to the model presented in  
 572 Section 5.1, QoS is presented in Fig. 8 as a function of  $P_{loss}$ , according to curve  
 573 related to the target GoP size (90 frames as per Table 1).

574 Fig. 8 also shows the curve calculated by using the real GoP size (56 frames as per  
 575 Table 4). The target size defines a lower bound for such a mapping because of its  
 576 higher value, which would translate into higher dependency among consecutive  
 577 frames, thus generating higher spatial error rates per given  $P_{loss}$ . Once such a  
 578 mapping is available, a further improvement can be achieved through learning-  
 579 based sender-side policies to be implemented: when no data are available, the  
 580 target GoP size can be used as a lower bound for QoE. Then, in the presence of  
 581 a feedback loop - common in video streaming scenarios - both the loss rate and  
 582 the GoP size can be estimated, in turn allowing for a finer tuning of the model  
 583 parameters. Such a mechanism can lead to a more efficient use of the network  
 584 links (for instance, using a subset of links) to optimise the use of resources while  
 585 contemporary satisfying the video quality objective.

586

### 587 5.3 Open Research Challenges

588 In this section, we briefly go through several open research challenges deriving  
 589 from this work and described in the literature. The first one, briefly mentioned  
 590 before, is related to video coding and to the possibility to leverage cross-layer  
 591 designs to improve the achievable performance level. Coding-aware and coding-  
 592 intrusive techniques [17] can be used in this regard. Coding-aware means that the  
 593 encoding parameters are sent down to the network layer, which chooses the net-  
 594 work path (i.e., a set of available links, in the case of multipath) that is expected  
 595 to target the desired QoE at the receiver. Contrarily, coding-intrusive means that  
 596 the application-layer encoding procedure is fed with networks statistics to adapt  
 597 the former to the latter. Coding-intrusive techniques are more used than coding-  
 598 aware ones, because single-link scenarios are commonly taken into account as  
 599 reference, but the use of multipath techniques opens to the greater potential of

600 coding-aware techniques for two main reasons: *(i)* any decisions taken at the ap-  
 601 plication layer will likely consider the link as a single (logical) one, thus forcing an  
 602 algorithm to rely on average values of the network statistics; instead, a decision  
 603 taken at the network layer can leverage the full knowledge of each link statistics,  
 604 thus opening to more targeted strategies. Furthermore, *(ii)* flexible strategies  
 605 at the network layer have the potential to provide better results in terms of  
 606 QoE - for the same reason as before - also when energy constraints are taken  
 607 into account, i.e., by respecting energy constraints while choosing the links. As  
 608 said before, coding-intrusive techniques require cross-layer approaches [48] and  
 609 more complexity hidden in the network layer. Achieving results similar to those  
 610 provided by coding-aware techniques can prove challenging, but can provide a  
 611 larger flexibility. Conceptually, it translates into multimedia-centric networking  
 612 as alternative to the more common network-centric one.

613 A further challenge that requires careful attention is the packet reception order  
 614 and the presence of a large number of duplicates - likely to occur if redundancy  
 615 is used with multipath/multihoming, as in our scenario - because it influences  
 616 how both duplicates and out-of-order packets are treated at the receiver [49].  
 617 For instance, in the case of the Gstreamer dejitter buffer, a certain number of  
 618 out-of-order packets can mislead the Gstreamer pipeline into forcing a so-called  
 619 *resync* (video jumping back in time) because of the erroneous (duplicated) SNs  
 620 at the receiver with respect to the expected ones. Such a phenomenon hampers  
 621 video continuity, and calls for optimised strategies at the receiver buffer, which  
 622 must guarantee both video continuity and low playout delay, two requirements  
 623 contrasting each other. In fact, video continuity would benefit of a larger buffer  
 624 accumulating packets and absorbing any interference due to the network, while  
 625 low playout delay dictates a very short buffer to reduce buffering as much as  
 626 possible. Because of this, novel strategies are needed to better handle the re-  
 627 quirements of critical real-time video streaming.

## 628 6 Conclusions

629 In this work, we have presented the results of a real testbed to deliver real-time  
 630 air-to-ground multimedia feeds. The use cases of interest are those involving the  
 631 use of UAVs in BVLoS conditions. We have presented an analytical framework to  
 632 model the error in a multihoming/multipath setup, leveraging multiple physical  
 633 channels, which in our scenario are represented by three cellular connections  
 634 to opportunistically use the networks of different ISPs. Network statistics have  
 635 been collected in the testbed to characterise QoS parameters of interest for a  
 636 real-time multimedia system, such as loss rate and error burst length, which are  
 637 used in our framework to demonstrate how the QoE can be improved at the GCS  
 638 thanks to multipath features. Network diversity plays an important role in this  
 639 scenario, and the more the diversity can be exploited, the more the QoE can be  
 640 improved; otherwise, the system provides a performance level equivalent to that  
 641 offered by the use of a single network link. The largest network diversity found  
 642 in our testbed is in the urban part of it. The framework we propose herein to



643 characterise a multipath channel is complemented by the analytical mapping of  
 644 QoS into QoE evaluations, and the measurements collected in the real testbed  
 645 have been used to show how a multihoming/multipath system, as the one herein  
 646 proposed, can be used to target a given QoE at the GCS. Given our objective to  
 647 improve the QoE at the receiver, we have shown how the MOS reported by the  
 648 UAV pilot is greater (or equal, at a minimum) to the MOS the same pilot reports  
 649 in the absence of multipath in both urban and suburban scenarios in the tests  
 650 we carried out. The improved QoE reported by the UAV pilot is confirmed by  
 651 computing PSNR and SSIM measurements on the received video feed. In future  
 652 works, we will consider the use of reinforcement learning to automatically adapt  
 653 the scheduling strategy to the network conditions.

## 654 References

- 655 1. X. Cao, P. Yang, M. Alzenad, X. Xi, D. Wu, and H. Yanikomeroglu, "Airborne  
 656 Communication Networks: a Survey," *IEEE Journal on Selected Areas in Commu-  
 657 nications*, vol. 36, no. 9, pp. 1907–1926, 2018.
- 658 2. M. Bacco, P. Barsocchi, P. Cassara, D. Germanese, A. Gotta, G. R. Leone, D. Mo-  
 659 roni, M. A. Pascali, and M. Tampucci, "Monitoring Ancient Buildings: Real De-  
 660 ployment of an IoT System Enhanced by UAVs and Virtual Reality," *IEEE Access*,  
 661 vol. 8, pp. 50 131–50 148, 2020.
- 662 3. N. Nomikos, E. T. Michailidis, P. Trakadas, D. Vouyioukas, H. Karl, J. Martrat,  
 663 T. Zahariadis, K. Papadopoulos, and S. Voliotis, "A UAV-based Moving 5G RAN  
 664 for Massive Connectivity of Mobile Users and IoT Devices," *Vehicular Communi-  
 665 cations*, vol. 25, p. 100250, 2020.
- 666 4. B. Alzahrani, O. S. Oubbati, A. Barnawi, M. Atiquzzaman, and D. Alghazzawi,  
 667 "UAV assistance paradigm: State-of-the-art in applications and challenges," *Jour-  
 668 nal of Network and Computer Applications*, vol. 166, p. 102706, 2020.
- 669 5. M. Bacco, S. Chessa, M. Di Benedetto, D. Fabbri, M. Girolami, A. Gotta, D. Mo-  
 670 roni, M. A. Pascali, and V. Pellegrini, "UAVs and UAV Swarms for Civilian Ap-  
 671 plications: Communications and Image Processing in the SCIADRO Project," in  
 672 *International Conference on Wireless and Satellite Systems*. Springer, 2017, pp.  
 673 115–124.
- 674 6. S. Bertrand, N. Raballand, F. Viguier, and F. Muller, "Ground Risk Assessment  
 675 for Long-Range Inspection Missions of Railways by UAVs," in *2017 International  
 676 Conference on Unmanned Aircraft Systems (ICUAS)*. IEEE, 2017, pp. 1343–1351.
- 677 7. N. Mohamed, J. Al-Jaroodi, I. Jawhar, A. Idries, and F. Mohammed, "Unmanned  
 678 Aerial Vehicles Applications in Future Smart Cities," *Technological Forecasting  
 679 and Social Change*, vol. 153, p. 119293, 2020.
- 680 8. R. Muzaffar, E. Yanmaz, C. Raffelsberger, C. Bettstetter, and A. Cavallaro, "Live  
 681 Multicast Video Streaming from Drones: an Experimental Study," *Autonomous  
 682 Robots*, vol. 44, no. 1, pp. 75–91, 2020.
- 683 9. S. Si-Mohammed, M. Bouaziz, H. Hellaoui, O. Bekkouche, A. Ksentini, T. Taleb,  
 684 L. Tomaszewski, T. Lutz, G. Srinivasan, T. Jarvet *et al.*, "Supporting Unmanned  
 685 Aerial Vehicle Services in 5G Networks: New High-Level Architecture Integrating  
 686 5G With U-Space," *IEEE Vehicular Technology Magazine*, 2020.
- 687 10. M. Bacco, P. Cassara, A. Gotta, and V. Pellegrini, "Real-Time Multipath Mul-  
 688 timedia Traffic in Cellular Networks for Command and Control Applications," in

- 689 *2019 IEEE 90th Vehicular Technology Conference (VTC2019-Fall)*. IEEE, 2019,  
690 pp. 1–5.
- 691 11. D. Cavaliere, S. Senatore, and V. Loia, “Proactive UAVs for cognitive Contextual  
692 Awareness,” *IEEE Systems Journal*, vol. 13, no. 3, pp. 3568–3579, 2018.
  - 693 12. A. A. Hodroj, M. Ibrahim, and Y. Hadjadj-Aoul, “A Survey on Video Streaming  
694 in Multipath and Multihomed Overlay Networks,” *IEEE Access*, 2021.
  - 695 13. M. Marchese, A. Moheddine, and F. Patrone, “IoT and UAV Integration in 5G  
696 Hybrid Terrestrial-Satellite Networks,” *Sensors*, vol. 19, no. 17, pp. 1–19, 2019.
  - 697 14. M. Bacco, A. Berton, A. Gotta, and L. Caviglione, “IEEE 802.15.4 Air-Ground  
698 UAV Communications in Smart Farming Scenarios,” *IEEE Communications Let-  
699 ters*, pp. 1–4, July 2018.
  - 700 15. X. Lin, V. Yajnanarayana, S. D. Muruganathan, S. Gao, H. Asplund, H.-L. Maat-  
701 tanen, M. Bergstrom, S. Euler, and Y.-P. E. Wang, “The Sky Is Not the Limit:  
702 LTE for Unmanned Aerial Vehicles,” *IEEE Communications Magazine*, vol. 56,  
703 no. 4, pp. 204–210, 2018.
  - 704 16. B. Van der Bergh, A. Chiumento, and S. Pollin, “LTE in the Sky: Trading Off  
705 Propagation Benefits with Interference Costs for Aerial Nodes,” *IEEE Communi-  
706 cations Magazine*, vol. 54, no. 5, pp. 44–50, 2016.
  - 707 17. S. Afzal, V. Testoni, C. E. Rothenberg, P. Kolan, and I. Bouazizi, “A Holistic  
708 Survey of Wireless Multipath Video Streaming,” *arXiv preprint arXiv:1906.06184*,  
709 2019.
  - 710 18. S. Barré, C. Paasch, and O. Bonaventure, “Multipath TCP: from Theory to Prac-  
711 tice,” in *International Conference on Research in Networking*. Springer, 2011, pp.  
712 444–457.
  - 713 19. V. Singh, S. Ahsan, and J. Ott, “MP RTP: Multipath Considerations for Real-Time  
714 Media,” in *Proceedings of the 4th ACM Multimedia Systems Conference*. ACM,  
715 2013, pp. 190–201.
  - 716 20. B. Kreith, V. Singh, and J. Ott, “FRAC TaL: FEC-based Rate Control for RTP,”  
717 in *Proceedings of the 25th ACM international conference on Multimedia*, 2017, pp.  
718 1363–1371.
  - 719 21. S. Zhang, W. Lei, W. Zhang, Y. Guan, and H. Li, “Congestion Control and Packet  
720 Scheduling for Multipath Real Time Video Streaming,” *IEEE Access*, vol. 7, pp.  
721 59 758–59 770, 2019.
  - 722 22. T. Viernickel, A. Froemmgen, A. Rizk, B. Koldehofe, and R. Steinmetz, “Multipath  
723 QUIC: a Deployable Multipath Transport Protocol,” in *2018 IEEE International  
724 Conference on Communications (ICC)*. IEEE, 2018, pp. 1–7.
  - 725 23. W. Zhang, W. Lei, and S. Zhang, “A Multipath Transport Scheme for Real-  
726 Time Multimedia Services based on Software-Defined Networking and Segment  
727 Routing,” *IEEE Access*, vol. 8, pp. 93 962–93 977, 2020.
  - 728 24. B. Wang, W. Wei, Z. Guo, and D. Towsley, “Multipath Live Streaming via TCP:  
729 Scheme, Performance and Benefits,” *ACM Transactions on Multimedia Computing,  
730 Communications, and Applications (TOMM)*, vol. 5, no. 3, p. 25, 2009.
  - 731 25. Y. Xing, K. Xue, Y. Zhang, J. Han, J. Li, J. Liu, and R. Li, “A Low-Latency  
732 MPTCP Scheduler for Live Video Streaming in Mobile Networks,” *IEEE Trans-  
733 actions on Wireless Communications*, 2021.
  - 734 26. M. Bacco, T. De Cola, G. Giambene, and A. Gotta, “Advances on Elastic Traffic  
735 via M2M Satellite User Terminals,” in *2015 International Symposium on Wireless  
736 Communication Systems (ISWCS)*. IEEE, 2015, pp. 226–230.
  - 737 27. J. Wu, C. Yuen, B. Cheng, Y. Yang, M. Wang, and J. Chen, “Bandwidth-Efficient  
738 Multipath Transport Protocol for Quality-Guaranteed Real-Time Video over Het-

- erogeneous Wireless Networks,” *IEEE Transactions on Communications*, vol. 64, no. 6, pp. 2477–2493, 2016.
28. S. Ferlin, S. Kucera, H. Claussen, and Ö. Alay, “MPTCP meets FEC: Supporting Latency-Sensitive Applications over Heterogeneous Networks,” *IEEE/ACM Transactions on Networking*, vol. 26, no. 5, pp. 2005–2018, 2018.
29. J. Wu, B. Cheng, M. Wang, and J. Chen, “Energy-Aware Concurrent Multipath Transfer for Real-Time Video Streaming over Heterogeneous Wireless Networks,” *IEEE Transactions on circuits and systems for video technology*, vol. 28, no. 8, pp. 2007–2023, 2017.
30. M. Bacco, P. Cassarà, M. Colucci, and A. Gotta, “Modeling Reliable M2M/IoT Traffic over Random Access Satellite Links in Non-Saturated Conditions,” *IEEE Journal on Selected Areas in Communications*, vol. 36, no. 5, pp. 1042–1051, 2018.
31. X. Xiao, W. Wang, T. Chen, Y. Cao, T. Jiang, and Q. Zhang, “Sensor-Augmented Neural Adaptive Bitrate Video Streaming on UAVs,” *IEEE Transactions on Multimedia*, vol. 22, no. 6, pp. 1567–1576, 2019.
32. G. Giambene, D. K. Luong, V. A. Le, T. de Cola, and M. Muhammad, “Transport Layer Performance Combining Multipath and Network Coding in Mobile Satellite Networks,” *International Journal of Satellite Communications and Networking*, vol. 35, no. 6, pp. 583–603, 2017.
33. I. W. Damaj, D. K. Serhal, L. A. Hamandi, R. N. Zantout, and H. T. Mouftah, “Connected and Autonomous Electric Vehicles: Quality of Experience Survey and Taxonomy,” *Vehicular Communications*, vol. 28, p. 100312, 2021.
34. U. Engelke and H.-j. Zepernik, “Perceptual-Based Quality Metrics for Image and Video Services: A Survey,” in *Next Generation Internet Networks Conference*. IEEE, May 2007, pp. 190–197.
35. M. Alreshoodi, E. Danish, J. Woods, A. Fernando, and C. De Alwis, “Prediction of Perceptual Quality for Mobile Video Using Fuzzy Inference Systems,” *Transactions on Consumer Electronics*, vol. 61, pp. 546–554, November 2015.
36. E. A. A. Riker, M. Mu, and S. Zeadally, “Real-time QoE Prediction for Multimedia Applications in Wireless Mesh Networks,” in *IEEE Int. Conference CCNC’12*, January 2012, pp. 592–596.
37. W. Zhang, W. Lei, S. Liu, and G. Li, “A General Framework of Multipath Transport System based on Application-Level Relay,” *Computer Communications*, vol. 51, pp. 70–80, 2014.
38. H. Kim, L. Mokdad, and J. Ben-Othman, “Designing UAV Surveillance Frameworks for Smart City and Extensive Ocean with Differential Perspectives,” *IEEE Communications Magazine*, vol. 56, no. 4, pp. 98–104, 2018.
39. M. Bacco, P. Cassarà, A. Gotta, and M. Puddu, “A Simulation Framework for QoE-Aware Real-Time Video Streaming in Multipath Scenarios,” in *International Conference on Ad-Hoc Networks and Wireless*. Springer, 2020, pp. 114–121.
40. H. Liu and M. El Zarki, “Performance of H.263 Video Transmission over Wireless Channels using Hybrid ARQ,” *IEEE Journal on Selected Areas in Communications*, vol. 15, no. 9, pp. 1775–1786, 1997.
41. N. Celandroni and A. Gotta, “Performance Analysis of Systematic Upper Layer FEC Codes and Interleaving in Land Mobile Satellite Channels,” *IEEE Transactions on Vehicular Technology*, vol. 60, no. 4, pp. 1887–1894, 2011.
42. Y. J. Liang, J. G. Apostolopoulos, and B. Girod, “Analysis of Packet Loss for Compressed Video: Effect of Burst Losses and Correlation between Error Frames,” *IEEE Transactions on Circuits and Systems for Video Technology*, vol. 18, no. 7, pp. 861–874, 2008.

- 789 43. J. Poncella, G. Gomez, A. Hierrezuelo, F. J. Lopez-Martinez, and M. Aamir, "Quality  
790 Assessment in 3G/4G Wireless Networks," *Business Media, Wireless Personal*  
791 *Communications*, vol. 76, pp. 363–377, November 2014.
- 792 44. V. F. Monteiro, D. A. Sousa, T. F. Maciel, F. R. M. Lima, E. B. Rodrigues, and  
793 F. R. P. Cavalcanti, "Radio Resource Allocation Framework for Quality of Expe-  
794 rience Optimization in Wireless Networks," *Network*, vol. 29, pp. 33–39, Novem-  
795 ber/December 2015.
- 796 45. M. Sidibe, H. Koumaras, I. Kofler, A. Mehaoua, A. Kourtis, and C. Timmerer, "A  
797 Novel Monitoring Architecture for Media Services Adaptation Based on Network  
798 QoS to Perceived QoS Mapping," *Signal, Image and Video Processing*, vol. 2, pp.  
799 307–320, October 2008.
- 800 46. C. L. H. Koumaras, A. Kourtis and C. Shieh, "A Theoretical Framework for End-  
801 to-End Video Quality Prediction of MPEG-based Sequences," in *IEE Int. Conf.*  
802 *on Networking and Services*, July 2007, pp. 1–5.
- 803 47. Z. Wang, A. C. Bovik, H. R. Sheikh, and E. P. Simoncelli, "Image Quality Assess-  
804 ment: from Error Visibility to Structural Similarity," *IEEE Transactions on Image*  
805 *Processing*, vol. 13, no. 4, pp. 600–612, 2004.
- 806 48. A. Aliyu, A. H. Abdullah, O. Kaiwartya, F. Ullah, U. M. Joda, and A. N. Hassan,  
807 "Multi-Path Video Streaming in Vehicular Communication: Approaches and chal-  
808 lenges," in *2017 6th ICT International Student Project Conference (ICT-ISPC)*.  
809 IEEE, 2017, pp. 1–4.
- 810 49. M. Radi, B. Dezfouli, K. A. Bakar, and M. Lee, "Multipath Routing in Wireless  
811 Sensor Networks: Survey and Research Challenges," *sensors*, vol. 12, no. 1, pp.  
812 650–685, 2012.